Comparison of Reduced Order Lithium-Ion Battery Models for Control Applications

C. Speltino, D. Di Domenico, G. Fiengo and A. Stefanopoulou

***Abstract*— Lithium-ion batteries are the core of new plug-in hybrid-electrical vehicles (PHEV) as well as considered in many 2nd generation hybrid electric vehicles (HEV). In most cases the lithium-ion battery performances play an important role in the vehicle energy management. As consequence, battery modeling is one of the most important tasks for hybrid and electrical vehicles control. Full order electrochemical models have to be simplified in order to make them compatible with estimation algorithms embedded in a real-time on-board electronic control unit. The battery model simplification has to be carried out accurately in order to achieve maximum computational cost reduction while ensuring the best model performance and reaching an efficient system management. In this paper two different reduced order models, based on the electrochemical laws, are compared both with simulation results and with experimental data collected from a 10 Ah lithium-ion battery. The reduced order models characteristics are analyzed and compared in relation to the specific control objective.**

GLOSSARY

Symbol	Name	Unit
i_e	electrolyte current density	A cm^{-2}
i_s	solid current density	A cm^{-2}
ϕ_e	electrolyte potential	V
ϕ_s	solid potential	V
c_e	electrolyte concentration	mol cm^{-3}
c_s	solid concentration	mol cm^{-3}
c_{se}	solid concentration at electrolyte interface	mol cm^{-3}
j^{Li}	Butler-Volmer current density	A cm^{-3}
θ_n	normalized solid concentration at anode	-
θ_p	normalized solid concentration at cathode	-
U	open circuit voltage	V
U_n	anode open circuit voltage	V
U_p	cathode open circuit voltage	V
η	overpotential	V
F	Faraday's number	C mol^{-1}
I	battery current	A
R	gas constant	J K^{-1} mol^{-1}
T	temperature	K

TABLE I
LITHIUM-ION MODEL NOMENCLATURE.

I. INTRODUCTION

In the past few years lithium-ion batteries became one of the most popular type of battery in many application fields, such as portable electronics or electric vehicles. In the automotive field, lithium-ion batteries are the core of energy source and storage. In most cases the lithium-ion battery performances play an important role for the energy efficiency of these vehicles, suffering often the stress of very high transient loads. The charge-discharge rate for the lithium-ion battery can vary from 1-2 C (1 C is a discharge at nominal battery capacity) to a very fast pulse discharge, i.e. 40 C - 50 C over a short period of about 10 s - 20 s [9]. In order to efficiently manage the battery systems in different operating conditions a precise estimation of li-ions concentrations and associated State of Charge (SOC) is necessary. Since measuring these quantities is not possible, a mathematical model is needed. Unfortunately, a dynamic model able to capture the electrochemical reaction dynamics is typically of very high order and complexity [1], [6], [12]. Nevertheless, such type of model is very important because it can be parameterized on experimental data and used as a baseline in order to obtain more manageable reduced order models of very low order. The reduced order models typically introduce several approximations [1], [7], [3], [10], [2]. Whereas on one hand the order reduction allows the model implementation into a real-time on-board electronic control unit, on the other hand the simplified models neglect some dynamics so that they cannot predict accurately the current-voltage behavior across different operating conditions. As consequence, the battery model simplification has to be carried out accurately in order to achieve maximum computational cost reduction while ensuring the best model performance and reaching an efficient system management. In this paper, two different reduced order models, presented in [10] and [2] and based on the full order electrochemical battery model developed by Wang *et al*. [13], are proposed and compared. The simulation results are compared with both full order electrochemical battery model and experimental data collected from a 10 Ah lithium-ion battery from POWERIZER. The comparison is performed taking into account slow rate and critical high rate current demand, so that both the transient and steady-state model behavior can be analyzed. In the following, the full order electrochemical model is presented and the reduced order models are derived and discussed. Then the current-voltage profiles, as predicted by the reduced models, are compared with the full order and, finally, a comparison with experimental data is performed. The results discussion and the conclusions end the paper.

Carmelo Speltino, Domenico Di Domenico and Giovanni Fiengo are with Dipartimento di Ingegneria, Università degli Studi del Sannio, Piazza Roma 21, 82100 Benevento. E-mail: {carmelo.speltino, domenico.didomenico, gifiengo}@unisannio.it

Anna Stefanopoulou is with Mechanical Engineering University of Michigan, Ann Arbor MI. E-mail: annastef@umich.edu.

II. BATTERY MODEL FORMULATION

A lithium-ion battery is composed of three principal parts: two porous electrodes, namely cathode (positive) and anode

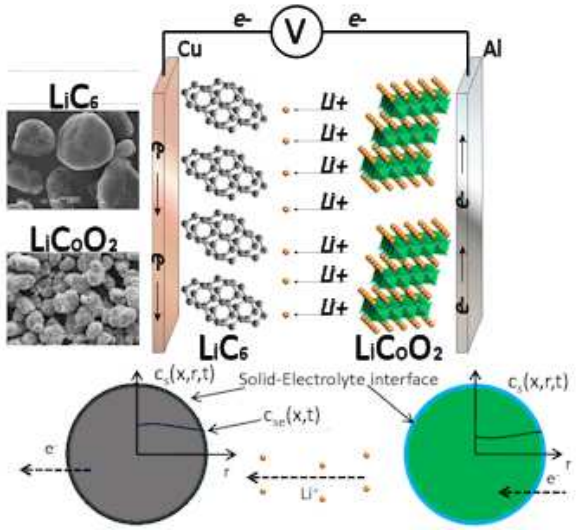

Fig. 1. Schematic macroscopic (x-direction) cell model with coupled microscopic (r-direction) solid diffusion model. The electrodes are filled with the electrolyte solution.

(negative) and an electrolyte solution that acts as separator between the electrodes as shown in Figure 1. During a discharge process, the lithium active particles diffuse up to the surface of the negative electrode where they react, producing lithium ions that flow through the electrolyte solution via diffusion and migration until they arrive at the positive electrode. The positively charged ions react with the metal oxide material particles of the positive electrode and diffuse within it. The electrons produced in the negative electrode reaction cannot flow through the electrolyte solution that acts as insulator and flow through an external circuit, producing the current. The inverse reactions occur during the battery charge. Due to their porous nature, the electrodes are represented as small spheres of active material along the electrode, with the chemical reactions occurring at the sphere surface [13]. The resulting Partial Differential Equations (PDE) describe the battery system with four quantities, i.e. solid and electrolyte concentrations (c_s, c_e) and solid and electrolyte potentials (ϕ_s, ϕ_e) [4], [9],

$$\frac{\partial}{\partial x}\left(\kappa^{eff}\overrightarrow{\nabla}_x\phi_e + \kappa_D^{eff}\overrightarrow{\nabla}_x \ln c_e\right) = -j^{Li} \tag{1}$$

$$\frac{\partial}{\partial x}\left(\sigma^{eff}\overrightarrow{\nabla}_x\phi_s\right) = j^{Li} \tag{2}$$

$$\frac{\partial \epsilon_e c_e}{\partial t} = \overrightarrow{\nabla}_x\left(D_e^{eff}\overrightarrow{\nabla}_x c_e\right) + \frac{1-t^0}{F}j^{Li} \tag{3}$$

$$\frac{\partial c_s}{\partial t} = \overrightarrow{\nabla}_r(D_s\overrightarrow{\nabla}c_s) \tag{4}$$

coupled with the Butler-Volmer current density equation

$$j^{Li}(x) = a_s j_0\left[\exp\left(\frac{\alpha_a F}{RT}\eta\right) - \exp\left(-\frac{\alpha_c F}{RT}\eta\right)\right] \tag{5}$$

where the overpotential η is obtained as

$$\eta = \phi_s - \phi_e - U(c_{se}) \tag{6}$$

where $U(c_{se})$ is the open circuit potential, which is an empirical correlation function of the solid concentrations and the coefficient j_0 calculated as

$$j_0 = k_0(c_e)^{\alpha_a}(c_{s,max} - c_{se})^{\alpha_a}(c_{se})^{\alpha_c}. \tag{7}$$

The cell potential is then computed as

$$V = \phi_s(x=L) - \phi_s(x=0) - \frac{R_f}{A}I \tag{8}$$

where R_f is the film resistance on the electrodes surface and A is the collectors surface. More details on the model and its parameters can be found in [9],[10], and [14].

A. Reduced Order Models

The first Electrode Averaged Model (EAM), derived in [3], can be achieved by neglecting the solid concentration distribution along the electrode and considering the material diffusion inside a representative solid material particle for each electrode. This introduces an average value of the solid concentration that can be related with the battery SOC. Furthermore, by assuming an high concentration of electrolyte material in the solution, the electrolyte concentration c_e can be considered constant and its average value can be used.

Although these simplifications result in a heavy loss of information, they can be useful in control and estimation applications as we demonstrate next. In accordance with the mean solid concentration, the spatial dependence of the Butler-Volmer current is ignored and a constant value $\bar{j}^{Li}$ is considered which satisfies the spacial integral (for the anode or the cathode)

$$\int_0^{\delta_n} j^{Li}(x)dx = \frac{I}{A} = \bar{j}_n^{Li}\delta_n \tag{9}$$

where δ_n is the anode thickness. This averaging procedure is equivalent to considering a representative solid material particle somewhere along the anode and the cathode [3].

The partial differential equation (4), describes the solid phase concentration along the radius of active particle, but the macroscopic model requires only the concentration at the electrolyte interface. By using the finite difference method for the spatial variable r, it is possible to express the spherical PDE into a set of ordinary differential equations (ODE), dividing the sphere radius in $M_r - 1$ slices, each of size $\Delta_r = \frac{R_s}{M_r - 1}$ and rewriting boundary conditions [8]. The new system presents $M_r - 1$ states $\mathbf{c_s} = (c_{s_1}, c_{s_2}, ...c_{s_{M_r-1}})^T$, representing radially distributed concentrations at finite element node points $1, ..., M_r - 1$

$$\dot{c}_s = \mathbf{A}c_s + \mathbf{B}\bar{j}^{Li}. \tag{10}$$

where $\mathbf{A}$ is a constant tri-diagonal matrix, function of the diffusion coefficient D_s. The output of the system is the value of the solid concentration at the sphere radius, that can be rewritten as

$$\bar{c}_{se} = c_{s_{M_r-1}} - \mathbf{D}\bar{j}^{Li}. \tag{11}$$

where $\mathbf{D}$ is function of diffusion coefficient D_s and active surface area a_s. Two sets of ODEs, one for the anode and one

for the cathode are then obtained. The positive and negative electrode dynamical systems differ at the constant values and at the input sign.

The initial values of $\bar{c}_{se}$ when the battery is fully charged is defined as $\bar{c}_{se,x}^{100\%}$ and when fully discharged as $\bar{c}_{se,x}^{0\%}$, with $x = p, n$ for the positive and negative electrode. It is convenient to define the normalized concentration, also known as stoichiometry, $\theta_x = \bar{c}_{se,x}/c_{se,max,x}$, with $x = p, n$ for the positive and negative electrode.

The battery voltage (8), using (6) and using the average values at the anode and the cathode, can be rewritten as

$$\begin{aligned} V(t) = (\bar{\eta}_p - \bar{\eta}_n) + \left(\bar{\phi}_{e,p} - \bar{\phi}_{e,n}\right) \\ + (U_p(\theta_p) - U_n(\theta_n)) - \frac{R_f}{A} I. \end{aligned} \tag{12}$$

Using the microscopic current average values and imposing the boundary conditions and the continuity at the interfaces, the solutions of equations (1) - (4) can be found. The results can be found in [10] and [3] and are not reported here for brevity.

Using (5) it is possible to express the overpotentials difference as function of average current densities and solid concentrations as follows

$$\bar{\eta}_p - \bar{\eta}_n = \frac{RT}{\alpha_a F} \ln \frac{\xi_p + \sqrt{\xi_p^2 + 1}}{\xi_n + \sqrt{\xi_n^2 + 1}} \tag{13}$$

where

$$\xi_p = \frac{\bar{j}_p^{Li}}{2 a_s j_{0p}} \quad \text{and} \quad \xi_n = \frac{\bar{j}_n^{Li}}{2 a_s j_{0n}}. \tag{14}$$

The approximate solution for the electrolyte potential at the interface with the collectors leads to

$$\bar{\phi}_{e,p} - \bar{\phi}_{e,n} = \phi_e(L) - \phi_e(0) = -\frac{I}{2Ak^{eff}} \left(\delta_n + 2\delta_{sep} + \delta_p\right). \tag{15}$$

Finally, the battery voltage (12) can be rewritten as a function of current demand and average solid concentration

$$\begin{aligned} V(t) = \frac{RT}{\alpha_a F} \ln \frac{\xi_p + \sqrt{\xi_p^2 + 1}}{\xi_n + \sqrt{\xi_n^2 + 1}} \\ + (U_p(\theta_p) - U_n(\theta_n)) - \frac{K_r}{A} I. \end{aligned} \tag{16}$$

where $K_r = \frac{1}{2Ak^{eff}} \left(\delta_n + 2\delta_{sep} + \delta_p\right) + R_f$ is a term that takes into account both internal and collector film resistances.

The second model reduction was introduced in [10] and will be here referred as State Values Model (SVM). The SVM reduction is performed by manipulating the governing equations in order to derive analytical transfer functions and later numerical transfer matrices describing the output response of the model variables $c_s(x,s), c_e(x,s), \phi_s(x,s), \phi_e(x,s)$ to an input current $I(s)$. Individual submodel responses are then combined in order to obtain the voltage response $V(s)$. Before manipulating the equations it is necessary to make the following assumptions:

- Linear model behavior
- Reaction current $j^{Li}(s)$ is decoupled from electrolyte concentration $c_e(x,s)$

Defining the dimensionless variable $z = x/\delta$, where $z = 0$ represents the current collector interface and $z = 1$ represents the separator interface, the solid phase charge concentration equation can be linearized and expressed as function of z

$$\frac{\sigma^{eff}}{\delta^2} \frac{\partial^2 \phi_s}{\partial z^2} - j^{Li} = 0 \tag{17}$$

with boundary conditions

$$-\frac{\sigma^{eff}}{\delta} \frac{\partial \phi_s}{\partial z}\bigg|_{z=0} = \frac{I}{A} \tag{18}$$

$$\frac{\partial \phi_s}{\partial z}\bigg|_{z=1} = 0 \tag{19}$$

and, in conformity with the second assumption, neglecting the 2nd term on the left hand side of the electrolyte charge concentration equation and assuming k^{eff} to be constant it is possible to express this equation as

$$\frac{k^{eff}}{\delta^2} \frac{\partial^2 \phi_e}{\partial z^2} + j^{Li} = 0 \tag{20}$$

with boundary conditions

$$\frac{k^{eff}}{\delta} \frac{\partial \phi_e}{\partial z}\bigg|_{z=1} = \frac{I}{A} \tag{21}$$

$$\frac{\partial \phi_e}{\partial z}\bigg|_{z=0} = 0. \tag{22}$$

Subtracting the corresponding equations it is possible to obtain a single static ODE that expresses the phase potential difference

$$\phi_{s-e} = \phi_s - \phi_e, \tag{23}$$

$$\frac{\partial^2 \phi_{s-e}}{\partial z^2} = \delta^2 \left(\frac{1}{k^{eff}} + \frac{1}{\sigma^{eff}}\right) j^{Li} \tag{24}$$

with boundary conditions

$$\frac{k^{eff}}{\delta} \frac{\partial \phi_{s-e}}{\partial z}\bigg|_{z=1} = -\frac{\sigma^{eff}}{\delta} \frac{\partial \phi_{s-e}}{\partial z}\bigg|_{z=0} = \frac{I}{A}. \tag{25}$$

Taking the Laplace transform of the conservation of lithium in the solid phase and solving it with respect to its boundary conditions, Jacobsen and West in [5] give the solid state diffusion

$$\frac{c_s(s)}{j^{Li}(s)} = \frac{1}{a_s F} \left(\frac{R_s}{D_s} \left[\frac{tanh(\beta)}{tanh(\beta) - \beta}\right]\right), \tag{26}$$

where $\beta = R_s (s/D_s)^{\frac{1}{2}}$, while the linearization of the Butler-Volmer equation yields

$$\eta = \frac{R_{ct}}{a_s} j^{Li} \tag{27}$$

where $R_{ct} = RT/[i_0 F(\alpha_a + \alpha_c)]$ is the charge transfer resistance. The battery voltage (8), using (6), can be expanded as

$$\begin{aligned} V(t) = \phi_e(L,t) - \phi_e(0,t) + \eta(L,t) - \eta(0,t) \\ + U_+(c_{s,e}(L,t)) - U_-(c_{s,e}(0,t)) - \frac{R_f}{A} I(t). \end{aligned} \tag{28}$$

After Laplace transform, the voltage response of the linear impedance model is

$$\frac{V(s)}{I(s)} = \frac{V_{OC}(s)}{I(s)} + \frac{V_{-}(s)}{I(s)} + \frac{V_{+}(s)}{I(s)} + \frac{V_{e}(s)}{I(s)} - \frac{R_f}{A}. \quad (29)$$

with individual terms arising due to bulk concentration, or open circuit voltage dynamics

$$\frac{V_{OC}(s)}{I(s)} = \frac{1}{AF}\left[\frac{\partial U_+}{\partial c_{s+}}\frac{1}{\delta_+ \epsilon_{s+}} - \frac{\partial U_-}{\partial c_{s-}}\frac{1}{\delta_- \epsilon_{s-}}\right]\frac{1}{s}, \quad (30)$$

negative and positive electrode solid state diffusion dynamics,

$$\frac{V_{-}(s)}{I(s)} = -\frac{\partial U_-}{\partial c_{s-}}\frac{\Delta c_{s,e-}(0,s)}{I(s)} - \frac{\eta_-(0,s)}{I(s)} + \frac{\Delta \phi_{e^-}^{j^{Li}}(L,s)}{I(s)}, \quad (31)$$

$$\frac{V_{+}(s)}{I(s)} = +\frac{\partial U_+}{\partial c_{s+}}\frac{\Delta c_{s,e+}(0,s)}{I(s)} + \frac{\eta_+(0,s)}{I(s)} + \frac{\Delta \phi_{e^+}^{j^{Li}}(L,s)}{I(s)}, \quad (32)$$

and electrolyte phase diffusion dynamics,

$$\frac{V_e(s)}{I(s)} = \frac{\Delta \phi_{e^+}^{\Delta c_e}(L,s)}{I(s)}. \quad (33)$$

Given a full order impedance model transfer matrix $y(s)/I(s)$, the reduced order transfer matrix is defined as

$$\frac{y^*(s)}{I(s)} = Z + \sum_{k=1}^{n} \frac{r_k s}{s - \lambda_k}. \quad (34)$$

In [10], λ_k and r_k are numerically generated eigenvalues and $n_x \times 1$ are residue vectors (obtained as in [11]) respectively. Z is obtained directly from full order model as $Z = \lim_{s\to 0} y(s)/I(s)$. Using the nth order parameters $(Z^T, \lambda_k, r_k^T)^T$ is possible to obtain the nth order time domain SVM

$$\begin{aligned} \dot{x}(t) &= Ax(t) + BI(t) \\ y^*(t) &= Cx(t) + DI(t) \end{aligned} \quad (35)$$

where

$$\begin{aligned} A = diag[\lambda_1 ... \lambda_n], B = [1...1]^T, \\ C = [r_1 \lambda_1 ... r_n \lambda_n], D = [Z + \textstyle\sum_{k=1}^{n} r_k]. \end{aligned} \quad (36)$$

The choice of model order is application dependent. In [10] a 5th order positive electrode, 5th order negative electrode and 1st order electrolyte model (later indicated as $5D_{s-}, 5D_{s+}, 1D_e$) has been chosen for testing in simulation, and its results are compared with the other reduced order model results. The model eigenvalues are

$$\begin{aligned} \lambda_- &= -[5.56 \times 10^{-3}, 6.05 \times 10^{-2}, 6.58 \times 10^{-1}, 6.38, 62.4] \\ \lambda_+ &= -[8.53 \times 10^{-3}, 6.08 \times 10^{-2}, 5.59 \times 10^{-1}, 5.82, 63.7] \\ \lambda_e &= -9.49 \times 10^{-1} \end{aligned} \quad (37)$$

including the open circuit potential submodel equation (30) with $\lambda_{OC} = 0$, the model is 12th order. Following typical convention SOC is defined as the fraction of capacity Q stored in the cell. Given an initial SOC at time $t = 0$ and assuming 100% columbic efficiency, SOC may be calculated as

$$SOC(t) = -\frac{1}{Q}\int_0^t I(t)dt. \quad (38)$$

As reported in [10] and [3] it is possible to express electrode bulk concentration as linear function of SOC,

$$c_{s,avg}(t) = [SOC(t)(\theta_{100\%} - \theta_{0\%}) + \theta_{0\%}]c_{s,max}. \quad (39)$$

Notice that the same equation, with equal stoichiometry parameters values, is used in the EAM model in order to obtain a SOC evaluation as a function of $c_{s,p}$. The SVM matrix C and D are then constructed linearizing the equations around 50% SOC, and substituting electrode bulk concentration with SOC as state variable.

III. Model Comparison

In order to compare EAM and SVM, several simulations have been performed with different current demand profiles. As in the linear SVM the matrix C and D depend on the initial value of SOC, a parameter identification procedure is necessary for every simulation tests at different operating conditions. It is important to note that the SVM presented here is an application of the SVM in [10] using linear parametrization techniques. Figure 2 shows the voltage output of the models to a current demand according to the FreedomCar Operation manual, consisting in a 30 A current discharge for 10 s followed by a 40 s rest and in a 22.5 A charge for 10 s followed by open circuit relaxation. Figure 3 shows the voltage error and the SOC prediction of the reduced order models. Table II highlights how both the models reproduce with a good accuracy the battery voltage. As the SVM evaluates the SOC based on a integrator, it is unable to predict the discontinuity on bulk concentration due to high current demand with fast dynamics.

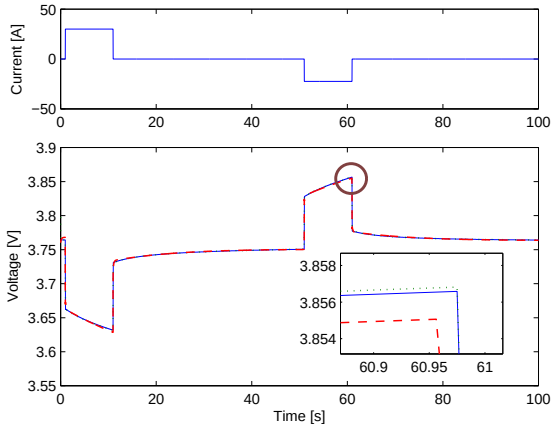

Fig. 2. Voltage response of complete and reduced order models under current demand profile as described in Freedom Car Manual. The voltage signals in bottom plot are respectively from Complete Model (solid blue line), EAM (dotted green line) and SVM (dashed red line)

Figures 4 and 5 show the performance of the models under high rate current demand. The profile is a series of 60A current pulse with the period equal to 10s, followed by 10s of relaxation. The results, reported in Table II, show a good voltage prediction compared to the complete model. As expected the linear SVM exhibits a greater error, in

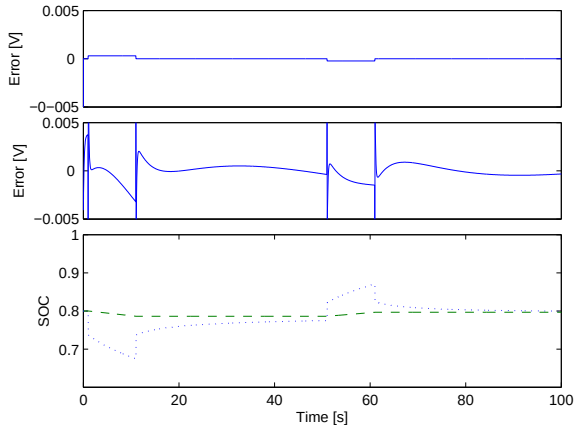

Fig. 3. Voltage error and SOC evaluation. From top, voltage error introduced by EAM, voltage error introduced by SVM and SOC evaluation (EAM (dotted blue line) and SVM (dashed green line))

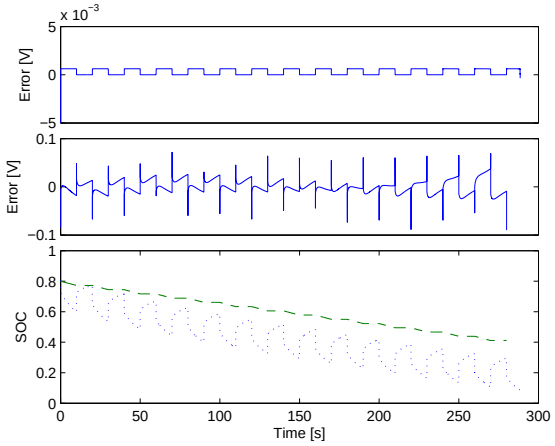

Fig. 5. Voltage error and SOC evaluation. From top, voltage error introduced by EAM, voltage error introduced by SVM and SOC evaluation (EAM (dotted blue line) and SVM (dashed green line))

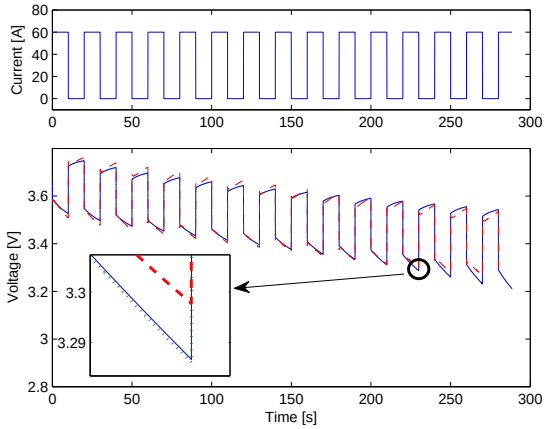

Fig. 4. Voltage response of complete and reduced order models under pulse current demand profile. The voltage signals in bottom plot are respectively from Complete Model (solid blue line), EAM (dotted green line) and SVM (dashed red line)

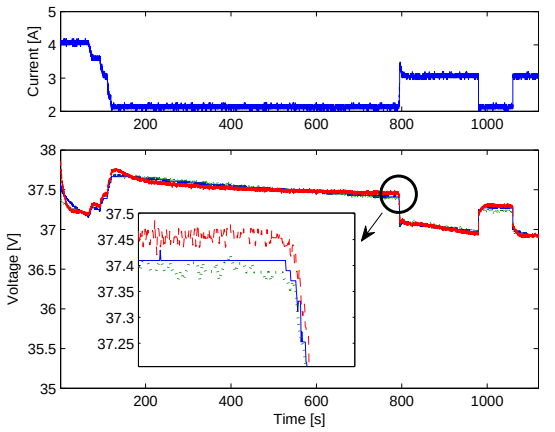

Fig. 6. Voltage response of identified reduced order models versus experimental data. The voltage signals in bottom plot are respectively from Battery Data (solid blue line), EAM (dotted green line) and SVM (dashed red line)

particular during the steps in current demand (the model parameters were identified supposing a 30A (3C) constant request, which imply an huge superimposed perturbation of $\pm$30A). An adaptive parameter update function of the current demanded can drastically reduce this error. Again, the main difference between the models is in SOC evaluation. The SVM predicts a final SOC approximately of 0.4, while EAM shows a nearly complete discharge, as expected by the experiments. This is because the integrator model only takes into account the average amount of current extracted from the battery, neglecting the high-rate depletion.

IV. Experimental Data Identification

The reduced order models exhibit a very low computational cost that allows not only a real time implementation but also the possibility of a parameter identification based on current-voltage profiles obtained from experimental data. An on-line parameters identification is particularly useful in order to have a device independent control and estimation system unit. In this paper, both the models have been identified off-line using several charge and discharge profiles collected with a 37 V - 10 Ah lithium-ion battery, and then validated on different data sets. The results reported in Figure 6 -7 show the voltage prediction of the two models during a selected experiment. The SVM appears to be more suitable for identification and exhibits a smaller error in voltage prediction if compared with the EAM, as confirmed by the results summarized in Table II. This is mainly due to the linearity of the model, in particular in the parameters dependence that leads to a very good model fit. On the contrary, EAM presents a non-linear structure and its dependence on the parameters is also non linear. On the other hand for the SVM there are a total of 24 parameters to identify, i.e. the 11 eigenvalues, C and D matrix and a static parameter function of initial SOC, while the EAM depends on just 9 parameters describing some

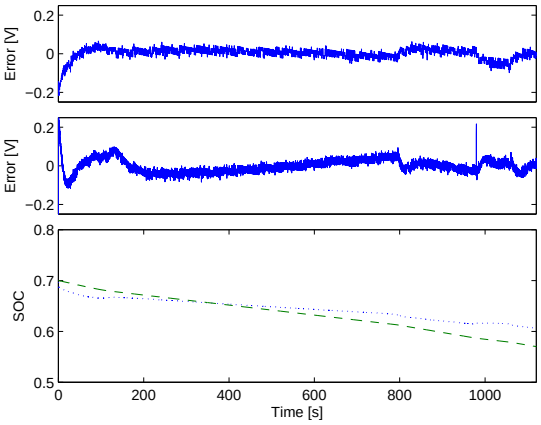

Fig. 7. Voltage error and SOC evaluation. From top, voltage error committed by EAM, voltage error committed by SVM and SOC evaluation (EAM (dotted blue line) and SVM (dashed green line))

physical battery properties. The big amount of parameters introduces in SVM an indetermination and may lead to errors in parameter identification if a poor or incomplete data set is used. To overcome this problem a partial subset of parameters was first identified and later the residual parameters were added gradually, removing the voltage prediction bias due to incorrect parameters identification. The SVM SOC evaluation still suffers the limitation due to its definition, and is again unable to predict discontinuities in electrode bulk concentration.

V. Conclusion

This paper describes two different reduced order models of a lithium-ion battery derived from a full order electrochemical model. While the full order model is able to predict electrochemical species and potential conservation distribution along the cell, the reduced orders are suited for real time application. As shown, both the models are able to predict voltage well, but they exhibit different backwards. The EAM model is mainly aimed to the SOC estimation, being able to take into account rapid electrode bulk concentration discontinuities and offering a highly precise voltage prediction with respect to the full order battery model and good performance with respect to the experimental data. Furthermore, the EAM depends on few parameters, and it is very simple to set-up because its initial conditions depend only on the battery SOC. Its main disadvantage is the strong non-linearity, in particular the non-linearity in the parameters dependence, which make an on-line parameters identification hard to implement and leads to a bigger error in voltage prediction. Conversely the SVM model presents a poor SOC estimation, unable to follow electrode bulk concentration during high transient but a very precise voltage prediction with respect to experimental data once all the parameters have been identified. Even if the model depends on a big amount of parameters and it is difficult to set up correctly, the simple linear structure of the model make it easy to identify and particularly suited for on-line adaptive control and battery voltage prediction.

Current Profile	Model	$E[\|error\|]$	$\max[\|error\|]$	Std σ
Simulation results				
8C discharge	EAM	$5.08e^{-4}$	$2.45e^{-2}$	$2.16e^{-4}$
	SVM	$2.2e^{-3}$	$2.14e^{-2}$	$3.2e^{-3}$
5C/10s pulse	EAM	$1.54e^{-4}$	$1.91e^{-3}$	$1.73e^{-4}$
	SVM	$6.5e^{-3}$	$3.69e^{-2}$	$8.0e^{-3}$
10C/10s pulse	EAM	$3.17e^{-4}$	$1.36e^{-3}$	$3.18e^{-4}$
	SVM	$1.02e^{-2}$	$8.96e^{-2}$	$1.33e^{-2}$
FreedomCar	EAM	$6.24e^{-5}$	$3.34e^{-2}$	$5.42e^{-4}$
	SVM	$9.72e^{-4}$	$2.01e^{-2}$	$1.6e^{-3}$
Experimental data fitting				
Val. profile 1	EAM	$2.77e^{-2}$	$7.93e^{-1}$	$3.64e^{-2}$
	SVM	$2.0e^{-2}$	$2.16e^{-1}$	$2.82e^{-2}$
Val. profile 2	EAM	$2.48e^{-2}$	$5.85e^{-1}$	$2.95e^{-2}$
	SVM	$1.87e^{-2}$	$2.05e^{-1}$	$2.32e^{-2}$

TABLE II

Analysis results. Error on voltage prediction.

References

[1] O. Barbarisi, F. Vasca, and L. Glielmo. State of charge kalman filter estimator for automotive batteries. *Control Engineering Practice*, 14:267 – 275, 2006.

[2] A. Stefanopoulou D. Di Domenico and G. Fiengo. Psm: Reduced order lithium-ion battery electrochemical model and extended kalman filter state of charge estimation. *ASME Journal of Dynamic Systems, Measurement and Control - Special Issue on Physical System Modeling*, 2008.

[3] D. Di Domenico, G. Fiengo, and A. Stefanopoulou. Lithium-ion battery state of charge estimation with a kalman filter based on a electrochemical model. *Proceedings of 2008 IEEE Conference on Control Applications*, 1:702 – 707, 2008.

[4] W.B. Gu and C.Y. Wang. Thermal and electrochemical coupled modeling of a lithium-ion cell. *Proceedings of the ECS*, 99:748–762, 2000.

[5] T. Jacobsen and K. West. Diffusion impedance in planar, cylindrical and spherical symmetry. *Electrochimica acta*, 40:255–262, 1995.

[6] J.A. Prins-Jansen, J.D. Fehribach, K. Hemmes, and J.H.W. de Wita. A three-phase homogeneous model for porous electrodes in molten-carbonate fuel cells. *J. Electrochem. Soc.*, 143:1617–1628, 1996.

[7] S. Santhanagopalan, Q. Guo, and R.E. White. Parameter estimation and model discrimination for a lithium-ion cell. *J. Electrochem. Soc.*, 154:A198–A206, 2007.

[8] W.E. Schiesser. *The Numerical Method of Lines: Integration of Partial Differential Equations*. Elsevier Science & Technology, 1991.

[9] K. Smith and C.Y. Wang. Solid-state diffusion limitations on pulse operation of a lithium-ion cell for hybrid electric vehicles. *Journal of Power Sources*, 161:628–639, 2006.

[10] K.A. Smith, C.D. Rahn, and C.Y. Wang. Control oriented 1d electrochemical model of lithium ion battery. *Energy Conversion and Management*, 48:2565–2578, 2007.

[11] Kandler A. Smith, Christopher D. Rahn, and Chao-Yang Wang. Model order reduction of 1d diffusion systems via residue grouping. *Journal of Dynamic Systems, Measurement, and Control*, 130, 2008.

[12] M.W. Verbrugge and B.J. Koch. Electrochemical analysis of lithiated graphite anodes. *J. Electrochem. Soc.*, 150:A374–A384, 2003.

[13] C.Y. Wang, W.B. Gu, and B.Y. Liaw. Micro-macroscopic coupled modeling of batteries and fuel cells. part i: Model development. *J. Electrochem. Soc.*, 145:3407–3417, 1998.

[14] C.Y. Wang, W.B. Gu, and B.Y. Liaw. Micro-macroscopic coupled modeling of batteries and fuel cells. part ii: Application to ni-cd and ni-mh cells. *J. Electrochem. Soc.*, 145:3418–3427, 1998.